RSC Advances

ROYAL SOCIETY OF CHEMISTRY

www.rsc.org/advances

Graphical and textual abstract

The micro/nano-strcuture composite SiO_2@Ag/AgCl was employed as a low cost photocatalyst for the degradation of RhB in aqueous solution under visible light irradiation, which exhibited excellent photocatalytic performance and stability.

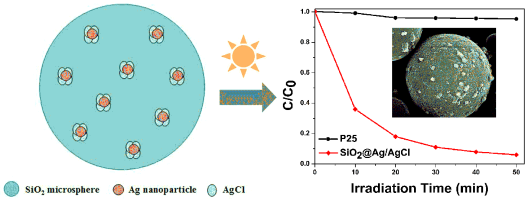

Cite this: DOI: 10.1039/c0xx00000x

www.rsc.org/xxxxxx

ARTICLE TYPE

SiO_2@Ag/AgCl: A low-cost and highly efficient plasmonic photocatalyst for degrading rhodamine B under visible light irradiation

Xuefeng Xu,[a] Man Wang,[a] Yanyan Pei,[a] Changchun Ai*[b] and Liangjie Yuan*[a]

Received (in XXX, XXX) Xth XXXXXXXXX 20XX, Accepted Xth XXXXXXXXX 20XX

DOI: 10.1039/b000000x

A series of highly efficient and low cost visible light-driven micro/nano-structure photocatalysts，composed of microstructure SiO_2 spheres and Ag/AgCl nanocomposites with different proportion of AgCl to Ag, have been facilely and controllably fabricated via deposition-precipitation method and in situ oxidation process. The obtained samples were characterized by X-ray diffraction (XRD), scanning electron microscopy (SEM), transmission electron microscopy (TEM), high-resolution transmission electron microscopy (HRTEM), energy dispersive spectrometry (EDS), X-ray photoelectron spectroscopy (XPS) and UV-vis diffuse reflectance spectra (UV-vis-DRS). The as-prepared photocatalysts exhibit wide absorption in the visible light region and display superior photocatalytic activity and excellent stability towards degradation of organic pollutants, *i.e.*, rhodamine B (RhB) compared with commercial TiO_2 (P25) and pure Ag/AgCl under visible light ($\lambda \geq 420$ nm). Furthermore, the molar ratio of AgCl to Ag in the SiO_2@Ag/AgCl composites has an important effect on their photocatalytic performance. The possible mechanism for the enhancement in decomposition of RhB molecules under visible light irradiation is discussed. This work may provide new insights into the fabrication of visible light-driven photocatalysts with low cost and excellent performance and facilitate their practical application in environmental issues.

1. Introduction

As the industrialization and globalization proceed, much attention has drawn on the environmental problems caused by organic contaminants and energy crisis.[1,2] Semiconductor photocatalysis based on harnessing and converting solar energy from sunlight into chemical energy has been considered not only as a “green” technology for environmental purification through degradation of environmental pollutants,[3,4] but also as a promising solution to solve the world wide energy crisis through hydrogen production by water splitting.[5,6] Among the various semiconductor photocatalysts, TiO_2 has been widely used because of its excellent photoelectric properties, non-toxicity, low cost and high stability.[7-10] However, its low utilization efficiency of solar energy with the absorbance of 4% of sunlight in ultraviolet (UV) region and relatively low photocatalytic efficiency caused by poor quantum efficiency limit its practical application.[11,12] Therefore, considerable efforts have been focused on the exploration and preparation of some novel visible-light-responded photocatalysts in order to make use of sunlight efficiently and improve the photocatalytic efficiency.[13]

Recently, plasmonic photocatalysts which combine the plasmon resonance of noble metal nanoparticles (such as sliver and gold) with a semiconductor catalyst,[14] are one of the most promising materials as high-performance visible-light-responded photocatalysts.[15,16] Typical plasmonic photocatalysts include Ag/AgX,[14,17-19] Ag/TiO_2,[20] Au/ZrO_2 and Au/SiO_2.[21] Among them, sliver/sliver halide composites have been widely investigated due to their outstanding photocatalytic activity and high stability in the degradation of pollutants under solar irradiation, which was first identified by Huang′ s group.[17,22-23] However, pure Ag/AgX has the tendency to agglomerate into larger particles and the surface area is low, which are not good for its photoactivity. Up to now, numerous works have been devoted to enhance the photocatalytic activity of pure Ag/AgX. Recently, Yao and Liu prepared a high-efficiency and stable Ag/AgCl@SiO_2 photocatalyst via coating a optically transparent SiO_2 layer on the surface of Ag/AgX.[24] Furthermore, Ag/AgX supported on substrates such as Al_2O_3,[25] BiOCl[26] and TiO_2[22] is also an effective method.[27] On the one hand, such supported Ag/AgX catalysts not only display excellent photocatalytic activity, but also keep optical stability to some extent.[27] On the other hand, the usage of the catalysts can be decreased and the cost can be reduced significantly since sliver as a noble metal leads to a high cost for application in industry.[28,29] Nevertheless, most of the current available photocatalysts require a centrifugation step to separate and recycle from the reaction system due to their small size in nanometer or submicrometer scale, which in turn increases the practical running cost.[30-32] Hence, many efforts have been focused on developing a high efficient and low cost photocatalyst with better recovery properties which could be available in practical application. Based on the discussions above, looking for a cheap and stable support material is the direct approach to both improving their performance and reducing cost.

In the present work, we report a facile and effective approach for

the synthesis of micro-SiO_2@nano-Ag/AgCl plasmonic photocatalyst with a low Ag content through deposition-precipitation and controllable in situ oxidation reaction. The photocatalytic activity of SiO_2@Ag/AgCl was evaluated in the degradation of Rhodamine B (RhB) under visible light irradiation. In addition, the correlation between photocatalytic activity and molar ratio of Ag^+:Ag^0 of the photocatalysts was discussed and the optimum ratio for the best photocatalytic activity was attained. The as-achieved micro/nano-structure photocatalysts exhibit excellent photocatalytic performance and durability towards decomposition of organics under visible light illumination, meanwhile, which can be easily separated from the reaction mixture and collected due to their micro-nanostructure and high density. The photocatalysts will have a potential application in wastewater treatment.

2. Experimental

2.1 Chemicals and Materials

N,N-dimethylformamide (DMF), polyvinylpyrrolidone (PVP, K30), sliver nitrate ($AgNO_3$), ferric chloride hexahydrate ($FeCl_3 \cdot 6H_2O$), triethanolamine (TEOA) and rhodamine B (RhB) were provided from Sinopharm Chemical Reagent Co., Ltd. Formaldehyde was obtained from Hubei University Chemical Plant. The micron-sized silica spheres were supplied by the Wuhan Shuaier Photo Electronic Materials Corporation, Ltd., which was synthesized according to Ai's method.[33] All the reagents used were of analytical or guarantee grade without additional purification. Deionized water was used in all the synthesis and treatment processes.

2.2 Incorporation of Sliver on Micro-sized silica sphere

Silver nanoparticles were incorporated on SiO_2 microspheres via a facile deposition-precipitation method. In a typical synthesis procedure, a certain amount of micro-sized SiO_2 were dispersed in 20 ml DMF and sonicated for 5 min. Then, the suspension was stirred magnetically for 1 h. 0.25 g of PVP was added to the vigorously stirred suspension and the result mixture was stirred for 4 h. In a separate beaker, a certain amount of TEOA was added to 50 ml of $AgNO_3$ aqueous solution (0.147 M) until the solution turned from turbid to clarify. And it was quickly added into above mixture under vigorous stirring for 3 h. The resulting mixture was yellowish in color and stood for overnight. In the presence of DMF and PVP, Ag^+ absorbed on the surface of micron silica spheres was incompletely reduced to Ag seeds. Then, 20 ml of 2% formalin solution was added as the reducing agent into above suspensions under stirring for one hour. The solution changed to dark colour, indicating the complete reduction of Ag^+. Finally, the particles were collected by filtration, and dried at 75 °C in a vacuum oven for 8 h.

2.3 Preparation of SiO_2@Ag/AgCl particles

The SiO_2@Ag/AgCl composite was synthesized through an in situ oxidation method. Typically, 1 g of SiO_2@Ag was dispersed into 150 ml of aqueous solution (PVP, 50 mM). Aqueous $FeCl_3$ (0.1 M) was slowly added to the above solution. After vigorous stirring for 2 h, the product was filtered, washed with water and ethanol (the solution pH was changed from 3 to 6 during the washing process), and dried in the dark. Different molar ratio of AgCl to Ag could be controlled through adjusting the amount of $FeCl_3$ (the total volume of $FeCl_3$ were 6.2 ml, 9.3 ml, 21.6 ml, 37.0 ml, respectively). The obtained powders were named as SAA-X (X=1, 2, 3, 4) corresponding to the molar ratio of $FeCl_3$:$AgNO_3$ at 1:1.5, 1:1, 2.33:1 and 4:1, respectively. For comparison, Ag/AgCl was synthesized using the similar processes, while the molar ratio of $FeCl_3$:$AgNO_3$ is 2.33:1. In addition, the SAA sample was dispersed in deionized water and then sonicated for 1 h to investigate the adhesion strength of Ag on SiO_2 microsphere.

2.4 Photocatalytic Performance

The photocatalytic performance of each SiO_2@Ag/AgCl composite was measured by the photocatalytic decomposition of organic dye rhodamine B (RhB) under visible light irradiation at ambient condition. In a typical procedure, 20 mg of photocatalysts were ultrasonically dispersed in a 50 ml aqueous solution of RhB (10 mg L^{-1}, pH=6), wherein a quartz tube was employed as the reactor. The dispersion was magnetically stirred in dark for 30 min to establish adsorption-desorption equilibrium of dyes on the surface of photocatalysts under room air-equilibrated conditions. Then, the photodegradation was carried out. The light source was a 500W Xe arc lamp (Changzhou Yuyu Lighting Co., Ltd.) equipped with an ultraviolet cutoff filter to provide visible light ($\lambda \geq 420$ nm) and focused onto the breaker. After visible light irradiation at regular time intervals, the absorbance of RhB dye was analyzed by a Shimadzu UV-3600 spectrophotometer. The visible-light photocatalytic performance of commercial TiO_2 and pure Ag/AgCl was also measured under the same conditions. To investigate the effect of solution pH on the degradation reaction, the pH of the reaction suspension were adjusted to 2 and 10 with HCl (1M) and NaOH (1M), respectively. For detecting the reactive species during photocatalytic reactivity, superoxide radical ($O^{2-\bullet}$), holes (h^+) and hydroxyl radicals ($HO^\bullet$) were investigated by adding 1.0 mM BQ (a quencher of $O^{2-\bullet}$), TEOA (a quencher of h^+) and IPA (a quencher of $HO^\bullet$), respectively.[40,41,45] The method was similar to the former photocatalytic activity test.

2.5 Sample Characterization

X-ray diffraction (XRD) patterns were obtained by a Bruker D8 advanced X-ray diffractometer with monochromated high-intensity Cu Kα radiation (λ=0.154056 nm) in a 2θ range of 10–90°. Images were obtained on a scanning electron microscopy (SEM, Zeiss Sigma FEI SEM) with energy-dispersive spectra and a transmission electron microscopy (TEM, JEOL JEM-100CX Ⅱ). X-ray photoelectron spectroscopy (XPS) was carried out on a Thermo Fisher ESCALAB 250Xi instrument with a monochromatic Al K Alpha (1486.68 eV) X-ray source, and the binding energies were referenced to the C1s line at 284.8 eV from adventitious carbon. The UV-vis absorption spectra (UV-vis) were measured with a Shimadzu UV-3600 spectrophotometer using $BaSO_4$ as the reference. The Brunauer-Emmett-Teller surface area (BET) was measured by a Gemini2390 system using N_2 adsorption/desorption at liquid-nitrogen temperature (77 K).

3. Result and discussion

3.1 Morphology and heterostructure of SiO_2@Ag/AgCl

The morphologies and structural characteristics of all samples were examined with SEM, TEM and HRTEM. SEM images of the SiO_2 microspheres, SiO_2@Ag and SiO_2@Ag/AgCl (SAA-3) are shown in Fig.1A, B, C, respectively. Compared to the other photocatalysts prepared, SAA-3 shows the best photocatalytic activity. SEM images of other samples were also taken, but no obvious changes were observed. Fig 1A shows that the support material micro-SiO_2 presented a sphere-like morphology with diameters of 2-3 μm. Fig. 1B illustrates that Ag nanoparticles in particulate shape with a size range from 80-120 nm are highly dispersed on surface of the micro-SiO_2 spheres. Fig. 1C suggests that the resultant SiO_2@Ag/AgCl shows a similar structure to that of the SiO_2@Ag precursor due to the formation of AgCl was an in situ oxidation process of metallic Ag on the SiO_2 surface. The surface of Ag nanoparticles has been almost completely covered by small AgCl crystals, forming an irregular bulk-like nanostructure. And the size of the Ag/AgCl particle increases to around 230 nm. The morphology of the SiO_2 substrate in the as-prepared composites is not changed compared to that of pure micro-SiO_2 spheres, that is, the SiO_2 microspheres are stable during the preparation process. In addition, Fig S1 shows the image of SiO_2@Ag/AgCl sample which has been sonicated for 1 h. It can be seen that the Ag/AgCl nanoparticles are firmly dispersed on the surface of SiO_2 spheres, indicating the strong adhesion of Ag on SiO_2 microsphere. For comparison, the SEM image of pure Ag/AgCl was shown in Fig S2, it can be seen that the particle size was range from 130-200 nm.

TEM images of SAA-3 are presented in Fig. 1D. As shown, Ag/AgCl nanoparticles are firmly attached on the surface of SiO_2 spheres. The particles display an irregular particulate structure with the crystalline size about 230 nm. Fig. 1E and F presents the corresponding HRTEM images of SAA-3. It can be seen that the determined lattice spacing of 0.201 nm matches with the values for cubic (200) phase (JCPDS 65-2871), indicating that Ag particles have deposited on the surface of SiO_2. The crystal lattice stripe of 0.325 nm is in good agreement with the (111) phase of cubic AgCl (JCPDS 31–1238). These results preliminarily indicate the possible formation of SiO_2@Ag/AgCl composites.

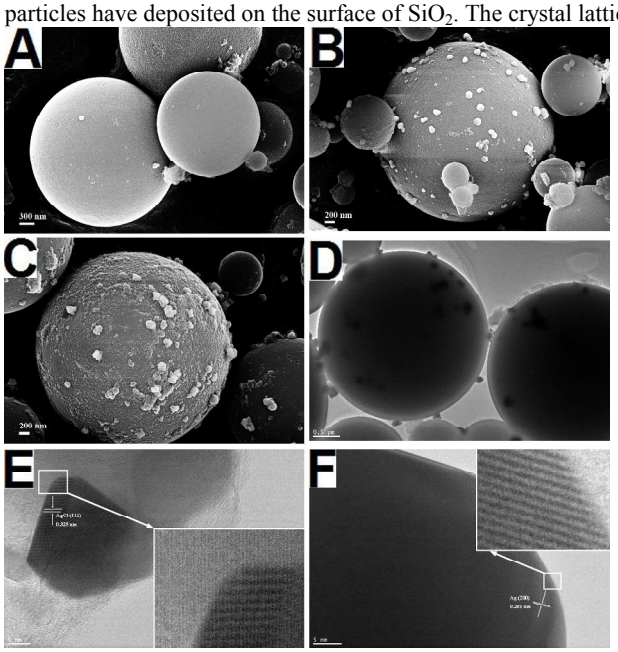

Fig. 1 SEM images of (A) SiO_2 microspheres, (B) SiO_2@Ag samples, (C) SiO_2@Ag/AgCl (SAA-3), (D) TEM images of SiO_2@Ag/AgCl (SAA-3),(E and F) HRTEM images of SiO_2@Ag/AgCl (SAA-3).

3.2 XRD Analysis

XRD patterns of SiO_2@Ag and SiO_2@Ag/AgCl composites synthesized with different atomic ratios of Ag^+/Ag^0 are shown in Figure 2. The broaden diffraction peak appeared at 23° in all samples is belonged to the amorphous silica matrix. For the SiO_2@Ag composite, the distinct diffraction peak (2θ) at 38.1°(111), 44.6°(200), 64.8°(220), 77.9°(311) are attributed to the typical cubic phase of Ag(JCPDS card no.65-2871), representing the formation of Ag particle on micro-SiO_2 spheres. After the oxidation reaction of SiO_2@Ag in $FeCl_3$ solution, the peaks(2θ) at 27.8°, 32.2°, 46.3°, 54.8°, 57.6°, 67.4° and 76.6° can be clearly observed ,which are ascribed to the (111), (200), (220), (311), (222), (400), (420) crystal planes of AgCl (JCPDS card no.31-1238). Simultaneously, the intensity of the peaks attributed to cubic Ag decreased significantly and almost can not be observed. It is possibly because the content of Ag is too low to be detected by XRD.[11,16] The existence of metallic Ag can be determined by the following SEM-EDS and XPS analysis.

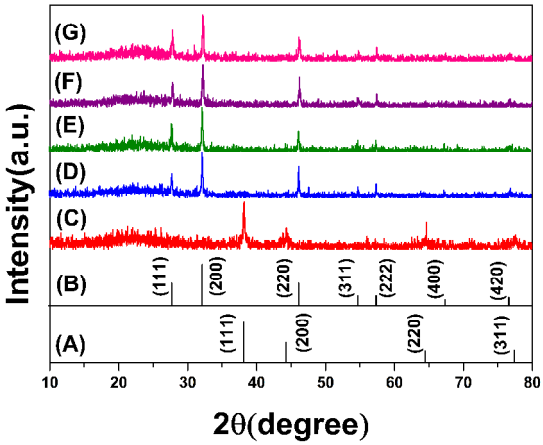

Fig. 2 X-ray diffraction patterns of (A) Ag (JCPDS file : 65-2871), (B)AgCl (JCPDS 31–1238),(C)pure SiO_2@Ag, (D) SAA-1, (E)SAA-2, (F) SAA-3 and (G)SAA-4 samples.

3.3 EDS and XPS Analysis

To verify the hybridization structure of the as-prepared samples, the element composition and the chemical state of their constituent elements were further investigated by EDS and XPS analysis in Fig. S3 and Fig. 3.

Fig. S3 shows the EDS data of all the photocatalysts fabricated with different Ag oxidation degree, and Si, O, Ag and Cl elements can be detected. It is obvious that the atomic percentage of silver is higher than that of chlorine in all samples, which suggests the coexistence of Ag/AgCl nanoparticles in the as-synthesized composites. The atomic ratio of Si and O is about 1:2, and the total content of Ag element is about 10 wt%. To further illustrate the oxidation degree of Ag in the SiO_2@Ag/AgCl, the atomic ratios of AgCl to Ag were calculated on the basis of EDS result, and the corresponding results are presented in Table 1. With the increase of the $FeCl_3$ amount, the atomic percentage of chlorine increases, since $FeCl_3$ provide the precursor for AgCl during the oxidation.

Table 1

Element composition of SiO_2@Ag/AgCl composites prepared by different molar ratios of Fe:Ag

Sample	Ag Content [a] (wt %)	$FeCl_3$:$AgNO_3$ (M/M)	Ag^+/Ag^0 [a] (M/M)
SAA-1	7.61	1:1.5	3.26
SAA-2	9.23	1:1	4.16
SAA-3	10.14	2.33:1	7.15
SAA-4	8.53	4:1	10.73

[a] Molar ratio from EDS

Fig. 3A displays the XPS spectrum of SAA-3, which also indicates that the SiO_2@Ag/AgCl composites are mainly composed of Si, O, Ag and Cl elements. Fig. 3B and C show the high-resolution XPS spectra of Ag 3d and Cl 2p in sample SAA-3, respectively. In figure 3B, two individual peaks at about 373.3 eV and 367.4 eV can be evidently observed, which may be assigned to the binding energies of Ag 3d 3/2 and Ag 3d 5/2, respectively.[34] The two bands can be further divided into two different peaks at 373.3 eV, 374.0 eV and 367.4, 367.9 eV, where those at 374.0 and 367.9 eV are attributed to the Ag^0 species, and those at 373.3 and 367.4 ev are ascribed to the Ag^+ in AgCl.[34] The XPS spectrum further confirms the existence of metallic Ag, agreeing with the XRD and EDS results.[26] In Fig. 3C, two peaks are presented at binding energies of about 197.6 and 199.3 eV, corresponding to Cl 2p3/2 and Cl 2p1/2 of AgCl, respectively, which are in consistent with reported values for AgCl.[23,29]

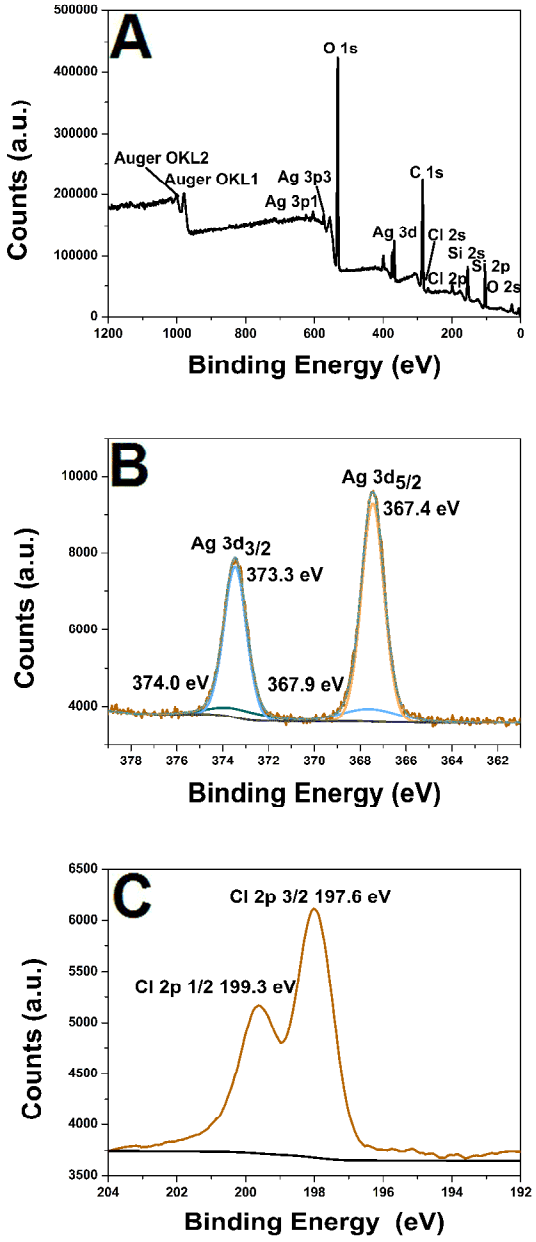

Fig. 3 XPS spectra of SiO_2@Ag/AgCl (SAA-3) sample. (A) survey scan spectrum, (B and C) high-resolution spectra of (B) Ag 3d and (C) Cl 2p.

3.4 UV−Vis Analysis

The optical properties of the as-prepared SiO_2@Ag/AgCl composites and reference samples (SiO_2, commercial TiO_2 and Ag/AgCl) were detected by UV-vis diffuse reflectance spectrum. As shown in Fig. 4, the spectrum of SiO_2 microspheres is transparent throughout the UV-vis light region. And the commercial TiO_2 only displays obvious absorption in the UV region but no absorption in the visible region. Compared with pure SiO_2 and commercial TiO_2, pure Ag/AgCl and SiO_2@Ag/AgCl both exhibit distinct absorptions both in UV and visible regions. The intense absorption at about 240 nm can be ascribed to the characteristic absorption of the AgCl semiconductor, the strong and broad absorption at a wavelength of 500 nm is attributed to the surface plasmon resonance of sliver nanoparticles on the surfaces of Ag/AgCl and SiO_2@Ag/AgCl.[14,35] As a result, the as-synthesised SiO_2@Ag/AgCl samples show strong light absorption in the whole visible-light region, thus they are favorable to the utilization of sunlight.

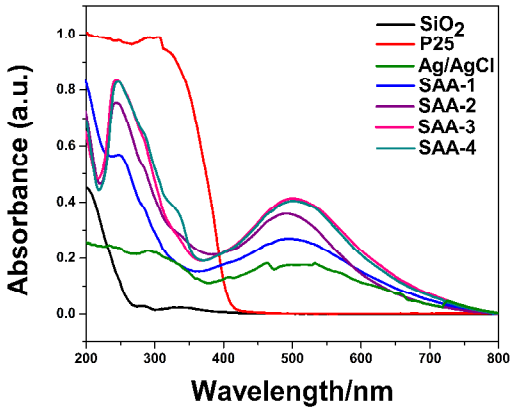

Fig. 4 UV-vis diffuse reflectance spectra of pure SiO_2, commercial TiO_2, Ag/AgCl, SAA-1, SAA-2, SAA-3 and SAA-4.

3.5 Photocatalytic Performance

The photocatalytic activity of the as-prepared SiO_2@Ag/AgCl with different atomic ratios of Ag^+: Ag^0 was investigated through monitoring the decomposition of Rhodamine B (RhB) solution with a concentration of 10 mg L^{-1} under visible-light irradiation ($\lambda \geq 420$ nm). For comparison, photocatalytic performance of commercial TiO_2 and pure Ag/AgCl were also examined under identical degradation conditions. Fig. 5A shows the temporal evolution of spectra changes of RhB dye photodegraded by SAA-

Cite this: DOI: 10.1039/c0xx00000x

www.rsc.org/xxxxxx

ARTICLE TYPE

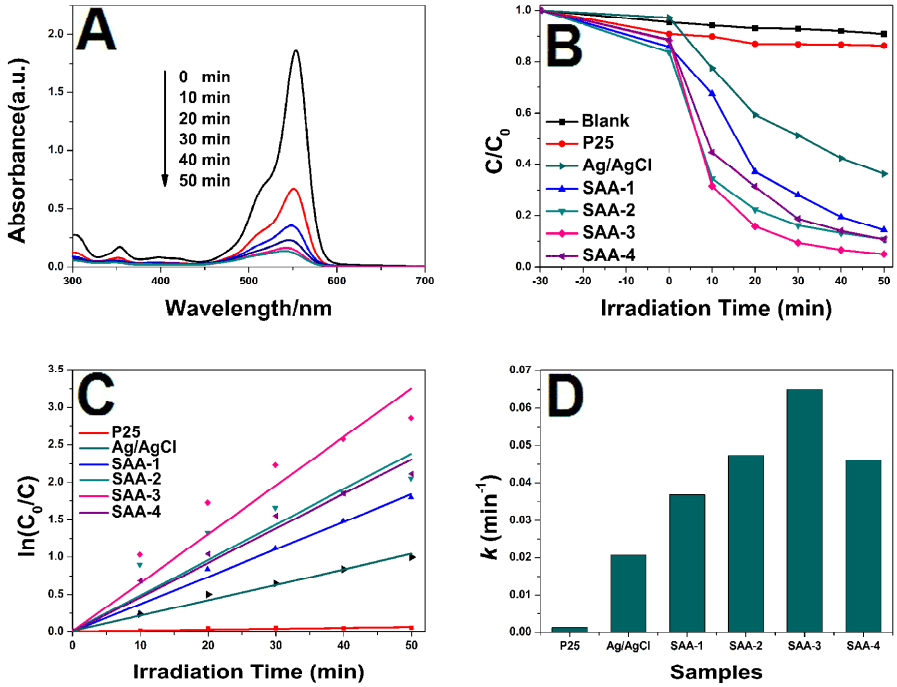

Fig. 5 (A) Temporal UV-vis absorption spectra for RhB solution in the presence of SAA-3 sample under visible light irradiation (λ≥420 nm), (B) photocatalytic degradation efficiencies of RhB over different photocatalysts under visible light irradiation (λ≥420 nm) , (C) kinetic linear simulation curves, in which C_0 is the concentration after absorption, and C is concentration at time t, (D) kinetic constants of the different photocatalysts for the degradation of RhB under visible light irradiation (λ≥420 nm).

3 under visible light irradiation. As shown, the peak intensity decreases apparently at wavelength of 554 nm as the irradiation time increases, accompanied with a slight blue shift. This phenomenon indicates the formation of a series of N-de-ethylated derivatives in a stepwise manner during the RhB degradation process.[36,37] More than 80% RhB dye can be decomposed within 20 min and eventually degraded completely after 50 min with the assistance of SiO_2@Ag/AgCl under the visible-light irradiation, indicating the excellent photocatalytic activity of the as-prepared sample.

The photodegradation dynamic curves of the RhB dye are displayed in Fig. 5B, in which C_0 represents the initial concentration of RhB and C represents the concentration at a given time. The adsorption capacity q_e of SAA-1, SAA-2, SAA-3, SAA-4 and pure Ag/AgCl are calculated as 3.38 mg/g, 3.92 mg/g, 2.76 mg/g, 2.68 mg/g and 0.22 mg/g according to the equation $q_e=(C_0-C_e)V/m$, in which C_e represents the concentration of RhB at the adsorption-desorption equilibrium, V represents the volume of dye solution and m represents the mass of photocatalysts. As shown, the self-photosensitized decomposition of RhB under visible light illumination in the absence of photocatalyst can be ignored. In comparison, the commercial TiO_2 shows negligible photodegradation of RhB, indicating that P25 has less efficient photocatalytic activity. The pure Ag/AgCl nanoparticles display limited photodecomposition ability with a degradation percentage of 63.8%, which may be the reason that the small specific surface area of pure Ag/AgCl nanoparticles is not beneficial to photocatalytic reaction. The degradation efficiency of RhB for SAA-1, SAA-2, SAA-3 and SAA-4 samples are 85.8%, 89.6%, 95.2% and 89.6% after irradiation for 50 min, respectively. Provided that the photocatalytic degradation of RhB on different catalysts follows an pseudo-first-order kinetics, $\ln(C_0/C)=kt$, where t is the reaction time and the k is the apparent reaction rate constant. As shown in Fig. 5C and D, the rate constants of SAA-1, SAA-2, SAA-3 and SAA-4 were evaluated as 0.03672 min^{-1}, 0.04742 min^{-1}, 0.06499 min^{-1} and 0.04613 min^{-1}, respectively, while, the rate constant of commercial P25 and pure Ag/AgCl was 0.0012 min^{-1} and 0.0207 min^{-1}, respectively. The rate constant (k) of SAA-3 was thus about 54.1 times and 3.2 times higher than that of P25 and pure Ag/AgCl, respectively. These results confirm that when being irradiated under visible light, all the as-prepared SiO_2@Ag/AgCl composites exhibit remarkable enhanced photodecomposition capacity than commercial TiO_2 and Ag/AgCl. It is worth noting that the photocatalytic efficiency of the SiO_2@Ag/AgCl samples increases with the increase of atomic ratio value of Ag^+:Ag^0 from 3.26-7.15, however, when the Ag^+/Ag^0 atomic ratio value up to 10.73, the photocatalytic activity decreases. Thus, it can be concluded that the photocatalytic performance is highly depended on the ratio of Ag^+ to Ag^0, and there should be an optimum ratio related to the best photocatalytic activity. For a fair comparison of all the SiO_2@Ag/AgCl photocatalysts, the ratio of the SAA-3 sample

may best approach the optimum one. The effect of the solution pH on the photocatalytic reaction has also been investigated. As shown in Fig S4, when the solution pH was 6 and 10, the degradation efficiencies of SAA-3 are almost equal, but the rate constant of SAA-3 at the pH of 10 is higher than that at the pH of 6. The degradation efficiency exhibit decrease when the solution pH was 2.

3.6 Mechanism of photocatalysis

The excellent photocatalytic performance of as-prepared SiO_2@Ag/AgCl photocatalysts and the interaction between Ag nanoparticles and AgCl crystals were further discussed from the following aspects. Firstly, sliver nanoparticles with SPR effect generated by the collective oscillations of the surface electrons make a contribution to the high visible light photocatalytic activity and stability.[12,28,38,39] The SPR of Ag NPs locates at the visible light region, which can enhance the absorption to the visible light and suppress the recombination of photoelectrons and holes.[12,17,40] Furthermore, the excellent conductivity of metallic Ag NPs is beneficial to the migration of interfacial charge and therefore avoid the recombination of electron-hole pairs efficiently.[12,28] Then they will be trapped by the adsorbed O_2 and H_2O to form active species, such as $O^{2-\bullet}$ and $HO^{\bullet}$. In order to investigate the main reactive species of the as-obtained SiO_2@Ag/AgCl samples involved in the photocatalytic reaction, some scavengers were used to scavenging the relevant active species during the photocatalytic process. As an $O^{2-\bullet}$ scavenger, benzoquinone (BQ) was added to the reaction system.[40,41,45] Triethanolamine (TEOA) was employed for scavenging h^+,[41] and isopropanol (IPA) was adopted to quench $HO^{\bullet}$.[41,45] As shown in Fig S5, the degradation efficiency of RhB decreases from 94.5% to 32% and 36.5% after adding TEOA and IPA, respectively, indicating that h^+ and $HO^{\bullet}$ are the main active species in the photocatalytic process. When BQ are added, the photocatalytic degradation efficiencies of dyes also decrease to 65.3%, suggesting that $O^{2-\bullet}$ also plays an important role in the photodegradation reaction. In summary, the main reactive species involved in the photocatalytic degradation of RhB are h^+, $HO^{\bullet}$ and $O^{2-\bullet}$. As for the as-prepared SiO_2@Ag/AgCl, when the catalysts in the dye solution were irradiated by visible light, a large amount of electron-hole(e^--h^+) pairs are generated in Ag NPs due to its SPR effect (as shown in Scheme 1). Then, the photoelectrons can be transferred to the ubiquitous molecular oxygen and then O^{2-} formed, followed by the generation of $HOO^{\bullet}$ radicals through protonation, and finally $HO^{\bullet}$ radicals are also formed.[28,42] All these reactive radical species contribute to the oxidation of the RhB dye molecule. Simultaneously, partial Ag^+ on the surface of AgCl NPs are reduced to Ag^0 species due to the visible light irradiation and the surface of AgCl particles is likely terminated by Cl^- anions, resulting in the negatively charged surface of AgCl NPs. Meanwhile, the electron distribution of the Ag NPs on the surface of AgCl can be polarized by AgCl, which would facilitate the electron-holes separation. The excited surface electrons on Ag NPs are far from the Ag/AgCl interface, and the holes are transferred to the AgCl surface corresponding to the oxidation of Cl^- to Cl^0.[17,23,42] Cl^0 is also the reactive radical species, which can oxidize RhB dye and then become reduced to Cl^- again. In this catalytic system, the oxidization of H_2O takes place simultaneously with the reduction of the Ag^+, in addition, the reduction of Cl^0 and the re-oxidation of Cl^- occurs during the reactions.[38,42] Therefore, the SiO_2@Ag/AgCl composite system can maintain stabilization in the whole photodegradation process. Once the amount of metallic Ag was very scarce, the enhancement of photocatalytic activity by SPR effect on the metallic sliver would be limited. But if AgNPs were excessive, some of the Ag NPs become the active sites accelerating the recombination of photoelectrons and holes, which would play a negative role on photocatalytic activity.[23,42,43] In addition, if the AgCl NPs were insufficient, the active species Cl^0 radicals may be reduced.[42] Secondly, the existence of surface OH groups can contribute to the photocatalytic reaction. As shown in the FTIR spectra of SiO_2 (Fig. S6), the broad absorption peak in the region of 3448 cm^{-1} is attributed to the O-H stretching mode of SiO_2 and water molecules, and the corresponding H-OH vibration appears at about 1631 cm^{-1}. Besides, the absorption peaks at 3700 and 897 cm^{-1} indicate the existence of Si-OH. It can be concluded that OH groups are located on the surface of SiO_2 spheres, and Zhao et al reported that surface OH groups can accept photoholes to form $HO^{\cdot}$ reactive radical species.[27,44] Thirdly, the specific surface area also plays an important role in determining the photocatalytic performance of a photocatalyst. As shown in the BET measurement (Fig. S7), the specific surface area value of SiO_2 was determined as 490.75 $m^2\ g^{-1}$ according to the computer calculation. And the specific surface area value of SAA-1, SAA-2, SAA-3, SAA-4 and pure Ag/AgCl are 377.09$m^2\ g^{-1}$, 382.32 $m^2\ g^{-1}$, 367.23 $m^2\ g^{-1}$, 348.15 $m^2\ g^{-1}$ and 1.67 $m^2\ g^{-1}$, respectively. The high surface area can enhance the absorption of organic dyes, which would help to concentrate dye molecules for the photoreactions.[32,45] Meanwhile, the high surface area provides the possibility for the efficient diffusion and transportation of absorbed organic molecules and hydroxyl radicals in photochemical reaction, which will enhance the photocatalytic activity of SiO_2@Ag/AgCl.[46,47] Finally, the micro/nano-structure of the as-prepared photocatalysts can offer more active absorption sites and photocatalytic reaction centers, which would improve the photodegradation efficiency.[2]

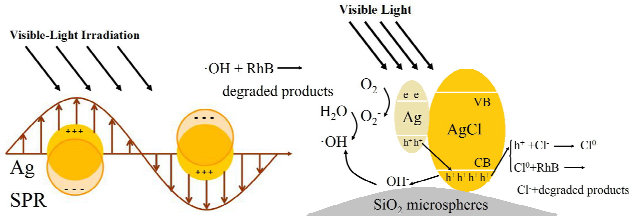

Scheme 1 Schematic diagram illustrating the possible photocatalytic mechanism of SiO_2@Ag/AgCl composites.

3.7 Stability and reusability of the as-prepared photocatalysts

Considering practical applications, stability and reusability of the photocatalyst have also been investigated. The stability of SAA-3 and pure Ag/AgCl have been investigated by recycling them in decomposing fresh RhB solution repeatedly under identical conditions. When the reaction finished, SAA-3 and pure Ag/AgCl were collected by filtration and centrifugation, respectively, then reused in another new catalytic reaction. Actually, the SAA powders almost deposited completely after the 20 min standing and the solution became clear. As shown in Fig. 6A, the photocatalytic efficiency of SAA-3 only exhibits a slight decrease,

Cite this: DOI: 10.1039/c0xx00000x

www.rsc.org/xxxxxx

ARTICLE TYPE

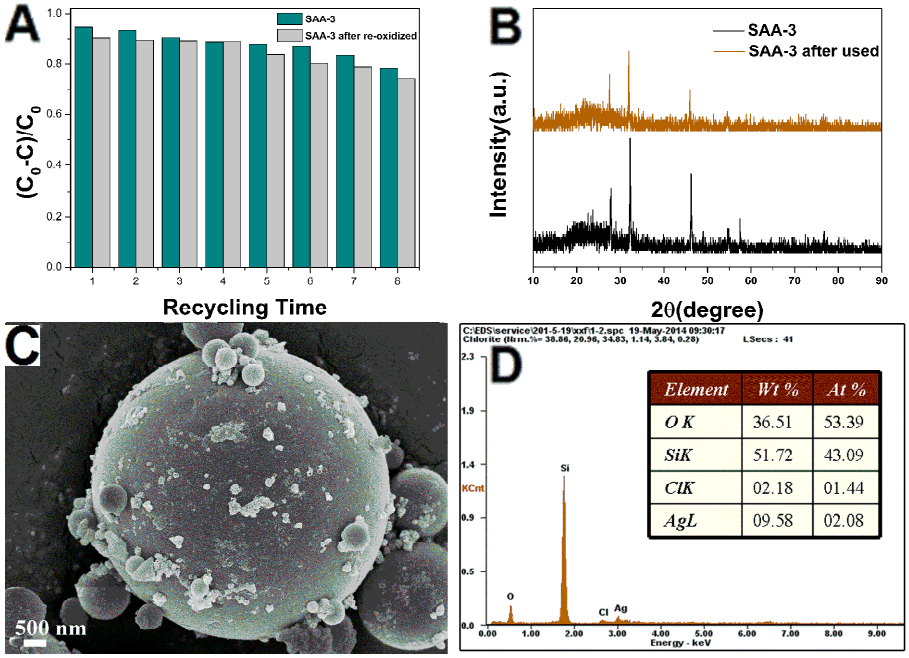

Fig. 6 (A) Eight cycling experiments results of SiO_2@Ag/AgCl (SAA-3), (B) XRD patterns of SiO_2@Ag/AgCl (SAA-3) before and after use, (C) SEM images and (D) EDS spectra of SiO_2@Ag/AgCl (SAA-3) photocatalyst after photocatalytic reaction.

although it was used 8 times continuously. However, Fig S8 shows that the photocatalytic activity of pure Ag/AgCl decreases noticeably after 3 runs recycling experiments, indicating that SiO_2 microspheres could improve the stability of Ag/AgCl. Moreover, the crystal phase, morphology and chemical composition of the reused photocatalyst after photocatalytic reaction have been studied. From the XRD analysis in Fig. 6B, it can be seen that the peak intensity of AgCl decreased after 8 runs recycling experiments compared to those of fresh samples. The SEM result in Fig. 6C reveals that although the photocatalytic activity decreases noticeably, the morphology of the photocatalyst does not display significant change after the recycling experiments, demonstrating that the micro/nano-structure of the composite is maintained well after circulation. According to the EDS data in Fig. 6D, the atomic ratio value of Ag^+ to Ag^0 is 7.15 before the photocatalytic recycling reaction, and it is 2.5 after the photocatalytic recycling reactions. However, the total Ag element content is almost constant. These results imply that parts of AgCl are decomposed to metallic Ag during the photocatalytic process, but the Ag content did not change. Therefore, the decrease of the photocatalytic activity may be ascribed to two reasons, namely the unavoidable catalyst loss during the recycling process and the partial decomposition of AgCl under the light irradiation.

The deactivated sample was re-oxidized by $FeCl_3$ solution, and it can be seen that the photocatalytic activity was completely recovered to its original value in Fig. 6A. During the second series of circulation test, the sample did not show significant loss of photocatalytic efficiency after 7 runs of the RhB degradation experiments, which suggests that the as-prepared photocatalyst has a promising capacity in industrial application according to the following consideration: firstly, the deactivated catalyst can be completely refreshed through mixing with $FeCl_3$ solution; secondly, our prepared composite is stable and can be reused for several times. Besides, the high efficient photocatalysts can be easily separated from the reaction mixture and collected because of its large size and high density; lastly, the preparation and re-oxidization process are both very mild and economic and the reagents are non-corrosive. Therefore, the reported SiO_2@Ag/AgCl ternary composites is a kind of efficient and stable visible-light-driven photocatalysts, which might serve as a promising candidate for the practical application in the degradation of pollutants.

4. Conclusion

In summary, a novel visible light driven plasmonic photocatalysts, composed of SiO_2 microspheres supported Ag/AgCl nanocomposites with low Ag loading content, were successfully synthesized by a two-step method involving a deposition-precipitation reaction followed by in situ oxidation. Their microstructure, chemical composition, optical properties, visible light-driven photocatalytic performance were investigated systematically. The as-prepared ternary composites could display high efficiency for decomposing organics under irradiation of visible light as compared to commercial TiO_2 and pure Ag/AgCl. It was also noted that the photocatalytic activity greatly depended on the ratio of AgCl:Ag and the photocatalyst with the ratio value

of 7.15 showed the highest photocatalytic performance. Moreover, the photocatalysts still kept a high level of catalytic activity even though it was used for eight times, which indicates that it has good recyclability and high optical stability under visible light irradiation. The enhanced photocatalytic performance of the photocatalysts can be attributed to profuse interface active sites due to its high surface areas and SPR effects of Ag NPs, which improve the efficiency of charge separation and make the catalysts stable. Considering the simple and mild preparation route, it is possible for the low cost photocatalyst with high activity and stability to be a promising material for practical application in environmental purification and water disinfection in industry.

Acknowledgement

This work was financially supported by National Natural Science Foundation of China (Grant No. 20171112 and Grant No. 21471119), and large scale Instrument and Equipment Sharing Foundation of Wuhan University (No. LF20110063).The author also would like to thank Prof. Ling Zan′s group (Wuhan University) for their instrument assistance in photocatalytic experiments.

Notes and references

[a] *College of Chemistry and Molecular Sciences, Wuhan University, Wuhan, China. Fax: +86-27-68752800; Tel: +86-13808661002; E-mail: ljyuan@whu.edu.cn*

[b] *School of Chemical Engineering & Pharmacy, Wuhan Institute of Technology, Wuhan, China. Fax: +86-27-68752800; Tel: +86-27-68752800; E-mail: aicchun@whu.edu.cn*

† Electronic Supplementary Information (ESI) available: [details of any supplementary information available should be included here]. See DOI: 10.1039/b000000x/

1 M. S. Zhu, P. L. Chen, W. H. Ma, B. Lei and M. H. Liu, *ACS Appl. Mater. Interfaces*, 2012, **4**, 6386-6392.

2 J. Y. Lei, W. Wang, M. X. Song, B. Dong, Z. Y. Li, C. Wang and L. J. Li, *Reactive & Functional Polymers*, 2011, **71**, 1071-1076.

3 Q. Zhang, D. Q. Lima, I. Lee, F. Zaera, M. F. Chi and Y. D. Yin, *Angew. Chem. Int. Ed*., 2011, **50**, 7088-7092.

4 D. V. Bavykin, J. M. Friedrich and P. C. Walsh, *Adv. Mater.*, 2006, **18**, 2807-2824.

5 A. Kudo and Y. Miseki, *Chem. Soc. Rev.*, 2009, **38**, 253-278.

6 W. Zhao, Y. L. Sun and F. N. Castellano, *J. Am. Chem. Soc.*, 2008, **130**, 12566-12567.

7 S. G. Kumar and K. S. R. K. Rao, *Nanoscale*, 2014, **6**, 11574-11632.

8 R. F. Dong, B. Z. Tian, C. Y. Zeng, T. Y. Li, T. T. Wang and J. L. Zhang, *J. Phys. Chem. C*, 2013, **117**, 213-220.

9 H. G. Yu, H. Irie and K. Hashimoto, *J. Am. Chem. Soc.*, 2010, **132**, 6898-6899.

10 K. Dai, L. H. Lu, J. Dong, Z. Y. Ji, G. P. Zhu, Q. Z. Liu, Z. L. Liu, Y. X. Zhang, P. L. Li and C. H. Liang, *Dalton Trans.*, 2013, **42**, 4657-4662.

11 G. Q. Luo, X. J. Jiang, M. J. Li, Q. Shen, L. M. Zhang and H. G. Yu, *ACS Appl. Mater. Interfaces*, 2013, **5**, 2161-2168.

12 L. Kuai, B. Y. Geng, X. T. Chen, Y. Y. Zhao and Y. C. Luo, *Langmuir*, 2010, **26**, 18723-18727.

13 S. G. Kumar and L. G. Devi, *J. Phys. Chem. A,* 2011, **115**, 13211-13241.

14 P. Wang, B. B. Huang, Z. Z. Lou, X. Y. Zhang, X. Y. Qin, Y. Dai, Z. K. Zheng and X. N. Wang, *Chem. Eur. J.*, 2010, **16**, 538-544.

15 W. S. Wang, H. Du, R. X. Wang, T. Wen and A. W. Xu, *Nanoscale*, 2013, **5**, 3315-3321.

16 Q. Zhu, W. S. Wang, L. Lin, G. Q. Gao, H. L. Guo, H. Du and A. W. Xu, *J. Phys. Chem. C*, 2013, **117**, 5894-5900.

17 P. Wang, B. B. Huang, X. Y. Qin, X. Y. Zhang, Y. Dai, J. Y. Wei and M. H. Whangbo, *Angew. Chem. Int. Ed.*, 2008, **47**, 7931-7933.

18 P. Wang, B. B. Huang, X. Y. Zhang, X. Y. Qin, H. Jin, Y. Dai, Z. Y. Wang, J. Y. Wei, J. Zhan, S. Y. Wang, J. P. Wang and M. H. Whangbo, *Chem. Eur. J.*, 2009, **15**, 1821-1824.

19 P. Wang, B. B. Huang, Q. Q. Zhang, X. Y. Zhang, X. Y. Qin, Y. Dai, J. Zhan, J. G. Yu, H. X. Liu and Z. Z. Lou, *Chem. Eur. J.*, 2010, **16**, 10042-10047.

20 Q. J. Xiang, J. G. Yu, B. Cheng and H. C. Ong, *Chem. Asian J.*, 2010, **5**, 1466-1474.

21 X. Chen, H. Y. Zhu, J. C. Zhao, Z. F. Zheng and X. P. Gao, *Angew.Chem.*, 2008, **120**, 5433-5436; *Angew. Chem. Int. Ed.*, 2008, **47**, 5353-5356.

22 X. P. Wang, Y. X. Tang, Z. Chen and T. T. Lim, *J. Mater. Chem.*, 2012, **22**, 23149-23158.

23 J, Jiang and L. Z. Zhang, *Chem. Eur. J.*, 2011, **17**, 3710-3717.

24 X. X. Yao and X. H. Liu, *Journal of Molecular Catalysis A: Chemical*, 2014, **393**, 30–38.

25 C. Hu, T. W. Peng, X. X. Hu, Y. L. Nie, X. F. Zhou, J. H. Qu and H. He, *J. Am. Chem. Soc.*, 2010, **132**, 857-862.

26 W. Xiong, Q. D. Zhao, X. Y. Li and D. K. Zhang, *Catalysis Communications*, 2011, **16**, 229-233.

27 H. Fan, J. Y. Zhu, J. C. Sun, S. X. Zhang and S. Y. Ai, *Chem. Eur. J.*, 2013, **19**, 2523-2530.

28 Y. Y. Zhao, L. Kuai and B. Y. Geng, *Catal. Sci. Technol.*, 2012, **2**, 1269-1274.

29 W. T. Liu, D. L. Chen, S. H. Yoo and S. O. Cho, *Nanotechnology*, 2013, **24**, 405706.

30 D. X. Huy, H. J. Lee, Y. B. Lee and W. S. Choi, *Journal of Colloid and Interface Science*, 2014, **425**, 178-185.

31 Y. Hou, X. Y. Li, Q. D. Zhao, G. H. Chen and C. L. Raston, *Environ. Sci. Technol.*, 2012, **46**, 4042-4050.

32 J. F. Guo, B. Ma, A. Y. Yin, K. N. Fan and W. L. Dai, *Applied Catalysis B: Environmental*, 2011, **101**, 580-586.

33 C.C. Ai, Y. Xiao, W. Wen and L.J. Yuan, *Powder Technol.*, 2011, **210**, 323-327.

34 M. S. Zhu, P. L. Chen and M. H. Liu, *J. Mater. Chem.*, 2011, **21**, 16413-16419.

35 P. Hu, X. L. Hu, C. J. Chen, D. F. Hou and Y. H. Huang, *CrystEngComm*,2014, **16**, 649-653.

36 H. G. Fu, S. C. Zhang, T. G. Xu, Y. F. Zhu and J. M. Chen, *Environ. Sci. Technol.*, 2008, **42**, 2085-2091.

37 W. J. Li, D. Z. Li, S. G. Meng, W. Chen, X. Z. Fu and Y. Shao, *Environ. Sci. Technol.*, 2011, **45**, 2987-2993.

38 R. C. Jin, Y. W. Cao, C. A. Mirkin, K. L. Kelly, G. C. Schatz and J. G. Zheng, *Science,* 2001, **294**, 1901-1903.

39 S. Link and M. A. El-Sayed, *J. Phys. Chem. B.*, 1999, **103**, 8410-8426.

40 C. H. An, X. J. Ming, J. Z. Wang and S. T. Wang, *J. Mater. Chem.*, 2012, **22**, 5171-5176.

41 S. F. Chen, L. Ji, W. M. Tang and X. L. Fu, *Dalton Trans.*, 2013, **42**, 10759-10768.

42 B. Ma, J. F. Guo, W. L. Dai and K. N. Fan, *Applied Catalysis B: Environmental*, 2013, **130**, 257-263.

43 B. Ma, J. F. Guo, W. L. Dai and K. N. Fan, *Applied Catalysis B: Environmental*, 2012, **123**, 193-199.

44 Y. F. Zhao, S. T. Zhang, B. Li, H. Yan, S. He, L. Tian, W. Y. Shi, J. Ma, M. Wei, D. G. Evans and X. Duan, *Chem. Eur. J.*, 2011, **17**, 13175-13181.

45 C. Dong, K. L. Wu, X. W. Wei, X. Z. Li, L. Liu, T. H. Ding, J. Wang and Y. Ye, *CrystEngComm*, 2014, **16**, 730-736.

46 J. G. Hou, Z. Wang, C. Yang, W. L. Zhou, S. Q. Jiao and H. M. Zhu, *J. Phys. Chem. C*, 2013, **117**, 5132-5141.

47 J. G. Hou, C. Yang, Z. Wang, Q. H. Ji, Y. T. Li, G. C. Huang, S. Q. Jiao and H. M. Zhu, *Applied Catalysis B: Environmental*, 2013, **142**, 579-589.